Use of LIDAR-derived images for mapping old landslides under forest

M. Van Den Eeckhaut,[1,2,*] J. Poesen,[1] G. Verstraeten,[1,2] V. Vanacker,[3] J. Nyssen,[1] J. Moeyersons,[4] L. P. H. van Beek[5] and L. Vandekerckhove[6]

[1] *Physical and Regional Geography Research Group, K.U. Leuven, Belgium*
[2] *Fund for Scientific Research, Flanders, Belgium*
[3] *Geography Department, U.C.L., Belgium*
[4] *Royal Museum for Central Africa, Tervuren, Belgium*
[5] *Department of Physical Geography, Utrecht University, The Netherlands*
[6] *Land Division, Ministry of Flanders, Belgium*

Correspondence to: M. Van Den Eeckhaut, Physical and Regional Geography Research Group, K. U. Leuven, Celestijnenlaan 200E B-3001 Heverlee, Belgium. E-mail: Miet.vandeneeckhaut@ geo.kuleuven.be

Abstract

Large, deep-seated landslides are common features in the Flemish Ardennes (Belgium). As most of these old (>100 years) landslides are located under forest in this hilly region, aerial photograph interpretation is not an appropriate landslide mapping method. This study tested the potential of LIDAR (Light Detection and Ranging) images for mapping old landslides under forest. Landslide inventory maps were created for a 125 km^2 area by applying the expert knowledge of seven geomorphologists to LIDAR-derived hillshade, slope and contour line maps in a GIS environment. Each of the seven LIDAR-based landslide inventories was compared (i) with the other six, (ii) with a detailed field survey-based inventory, and (iii) with a comparable study in which topographic data were extracted from a topographical map. The combination of the percentage of field landslides indicated by an expert and the percentage of positional discrepancies (expressed in terms of positional mismatch) were used to evaluate the quality of the LIDAR-based inventory maps. High-quality LIDAR-derived landslide inventory maps contain more than 70 per cent of the landslides mapped during the field survey, and have positional discrepancies smaller than 70 per cent when compared with the field survey-based inventory map. Four experts and the combination map of all experts satisfied these criteria. Together the seven experts indicated all landslides mapped in the field. Importantly, LIDAR enabled the experts to find ten new landslides and to correct the boundaries of eleven (of the 77) landslides mapped during the field survey. Hence, this study showed that large-scale LIDAR-derived maps analysed by experienced geomorphologists can significantly improve field survey-based inventories of landslides with a subdued morphology in hilly regions. Copyright © 2006 John Wiley & Sons, Ltd.

Keywords: old, deep-seated landslides; landslide inventory map; LIDAR; expert knowledge; hillshade map

Introduction

The Flemish Ardennes is a hilly region marked by old, large, deep-seated landslides (Vanmaercke-Gottigny, 1980; Ost *et al.*, 2003; Van Den Eeckhaut *et al.*, 2005). In this study, large, deep-seated landslides have an affected area of at least 1 ha and an assumed shear plane depth of more than 3 m. Although none of the landslides in the study area are dated, they are assumed to be older than 100 years because no historical documents are found describing their initiation. Due to the vicinity of cities such as Brussels and Ghent (Figure 1), the forested hills of the Flemish Ardennes have become attractive residential areas, and it appears that the expansion of settlements and human interference have increased vulnerability to landsliding. Indeed, reactivations of old landslides, causing damage to public and private property, have been documented, mostly during winter and spring after periods of persistent rainfall (e.g. in 1995 and 2002). This has resulted in an increased interest in the process of landsliding and its related problems by the local and regional authorities.
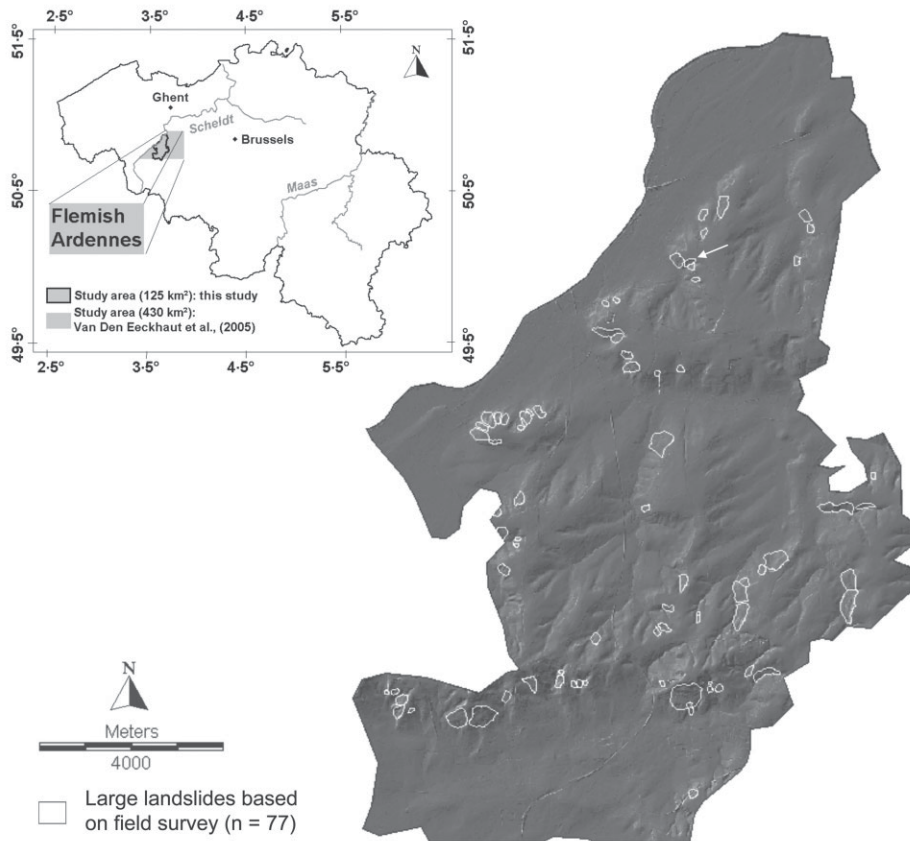
Figure 1. Location of the study area. The field survey-based landslides (*n* = 77) are shown on the LIDAR-derived hillshade map with sun elevation angle of 30° and sun azimuth angle of 315°. White arrow indicates landslide given to the experts as an example.

Optimal approaches to reduce landslide risk generally comprise a mix of four strategies (Schuster and Kockelman, 1996), among which reduction of development in landslide-prone areas, also known as avoidance (Crozier, 2005), is one of the most effective and economical. In order to apply the avoidance strategy in the Flemish Ardennes, the locations of landslide-prone areas must be known. As it is believed that past and present landslide locations are the key to prediction of future landslide locations (Carrara *et al.*, 1995; Zêzere, 2002), a detailed landslide inventory map is indispensable for the creation of landslide susceptibility maps (Ardizzone *et al.*, 2002; Vanacker *et al.*, 2003). These susceptibility maps allow the framing of rules linking land use regulations to the susceptibility zones.

For a 430 km² study area in the Flemish Ardennes, 135 large, deep-seated landslides were mapped at 1:10 000 scale during an intensive field survey (Ost *et al.*, 2003; Van Den Eeckhaut *et al.*, 2005). Afterwards the affected areas were digitized in a vector GIS (i.e. Mapinfo). Although time-consuming (*c.* 100 person-days) this technique was chosen because aerial photo interpretation (API), the most commonly used technique for regional landslide studies (Carrara *et al.*, 1992; van Westen *et al.*, 1999; Demoulin *et al.*, 2003; Metternicht *et al.*, 2005), did not result in an acceptable landslide inventory map. The poor results obtained by API in the Flemish Ardennes are due to the fact that 85 per cent of the landslides are partly or completely located under forest.

Recently, LIDAR data have become available for the Flemish Ardennes (DEM of Flanders, 2005), and this has raised the question as to whether this technology can be used to create reliable landslide inventories within forested areas. Therefore, the aim of this paper is to test the potential of LIDAR images for mapping old landslides under forest in hilly areas. The specific objectives are threefold: (1) to analyse the consistency of LIDAR-based landslide inventories produced by seven experts for a 125 km² test area; (2) to test the redundancy or complementarity of the combined use of LIDAR images and field surveys for the creation of landslide inventory maps; and (3) to compare our results with a study by Van Den Eeckhaut *et al.* (2005) in which topographical data were extracted from the contour lines on a topographical map.

Methods

Study area

Within the 430 km^2 study area investigated by Van Den Eeckhaut *et al.* (2005), a subarea of 125 km^2, representative of the Flemish Ardennes, was selected for use herein (Figure 1). The study region has a maritime temperate climate, with a mean annual rainfall of 800 mm, which is well distributed over all seasons. Its hilly character results from differential erosion of loose Tertiary and Quaternary sediments. The Tertiary sediments are characterized by an alternation of clayey sand layers and clay layers with a dip of less than 0·4 per cent to the NNE (Jacobs *et al.*, 1999). During the Quaternary, these layers were overlain by aeolian loess of varying thickness. Altitudes range from 10 m a.s.l. in the valley of the river Scheldt to 150 m a.s.l. on the hills. Hillslope gradients steeper than 0·20 m m^{-1} constitute only 2 per cent of the study area (Van Den Eeckhaut *et al.*, 2005). Most valleys are asymmetric with the steepest slope sections located on slopes facing south to northwest (Figure 1; Vanmaercke-Gottigny, 1995). The abundant presence of springs is characteristic for the Flemish Ardennes. Finally, land use depends on lithology, soil type, topography and hydrology pattern. Croplands are located on the plateaus of the lower hills and pastures dominate the hillslopes. The hills and the steepest hillslopes are forested (IWONL, 1987).

During the aforementioned field survey, Van Den Eeckhaut *et al.* (2005) mapped 77 large, deep-seated landslides in the selected 125 km^2 test area (Figure 1). An average large landslide has an affected area of 4·5 ha, is 200 m long, 210 m wide and is located on a south to northwest orientated slope section with an average slope gradient of 0·15 m m^{-1}. In total, 2·8 per cent of the study area is mapped as landslide-affected area, with 75 per cent of the landslides being partly or completely covered by dense forest. In the field, all landslides were classified using the system of Cruden and Varnes (1996) enlarged with a class for possible landslides as recommended by Guzzetti *et al.* (2000). The latter class contains doubtful sites having an unclear scarp. Deep-seated rotational earth slides dominate the study area accounting for 84 per cent (i.e. $n = 65$; Table I) of the mapped landslides. The remaining landslides are either classified as complex (i.e. $n = 4$) or possible (i.e. $n = 8$) landslides. The rotational and complex earth slides are further subdivided according to the freshness and preservation of the typical landslide characteristics. The terminology suggested by the International Association for Engineering Geology (IAEG) Commission on Landslides (1990) was used. To be classified as a type 1 rotational earth slide, a clear, high (>3 m) and rather steep main scarp, one or more reverse slopes which are responsible for the presence of an elongated pool parallel to the main scarp, and a convex foot must be present. When, due to erosion, the morphology of the reverse slopes had faded and changed into steps, landslides were classified as type 2. Type 3 landslides have a clear main scarp and a hummocky convex accumulation zone but they have no relicts of steps in the affected area.

LIDAR

Light Detection and Ranging or LIDAR is also known as laser altimetry or laser scanning (Gold, 2004). Essential elements of an airborne LIDAR mapping system are a scanning laser rangefinder, a differential Global Positioning System (GPS) and an inertial measurement unit (IMU; Haugerud *et al.*, 2003; Hodgson *et al.*, 2003). The rangefinder determines the distance to a target, and the GPS receiver and IMU provide for real-time spatial positioning of the aircraft in relation to the target (Gold, 2004). By combining all measurements, the altitude a.s.l. of the target is calculated. LIDAR is not a selective technique, meaning that not only altitudes of the soil surface are measured, but also altitudes of buildings and trees are included in the dataset (Hodgson *et al.*, 2003). To enable the creation of a so-called bare earth DEM, post-processing is necessary to separate ground returns from building and canopy returns.

Table I. Classification of the deep-seated (>3 m) landslides in the study area (see text for more information)

Class	Number of landslides	Freshness	Number of landslides
Rotational earth slide	65	Type 1	22
		Type 2	22
		Type 3	21
Complex earth slide (rotational earth	4	Type 1	1
slide with flow characteristics in accumulation zone)		Type 2	2
		Type 3	1
Possible landslide site	8		

After this separation there are in most cases enough ground returns left to create high-quality DEMs (Haneberg, 2005). Because LIDAR virtually sees through vegetation, it is, in contrast to photogrammetry, capable of high resolution topographic mapping of forested terrain (Haugerud *et al*., 2003).

In recent years, LIDAR has become a promising method in landslide research (Carter *et al*., 2001; Haugerud *et al*., 2003; Rowlands *et al*., 2003; Gold, 2004; McKean and Roering, 2004; Schulz, 2004; Haneberg, 2005; Haneberg *et al*., 2005; Glenn *et al*., 2006) and other geomorphological studies (White and Wang, 2003; Thoma *et al*., 2005). Using LIDAR-derived hillshade maps of a forested area near Seattle, Washington, Haugerud *et al*. (2003) developed a landslide inventory identifying twice as many deep-seated landslides in comparison with an inventory created from API. Close to this site, Schulz (2004) used LIDAR to improve an existing landslide inventory containing landslides reported to governmental agencies or mapped from aerial photographs, by adding previously unreported prehistoric landslides, which were not visible on aerial photographs due to their location under forest. The improved inventory, achieved by using the wider range of derivatives (i.e. slope, contour line and hillshade maps, and slope profiles) offered by LIDAR relative to API, showed four times more landslides than before. However, not all landslide parts could be delineated with the same accuracy: the location of the main scarp was mapped with relative certainty, the lateral margins with less certainty and the toes with a significant degree of uncertainty (Schulz, 2004). This difference in accuracy was not a shortcoming of LIDAR, but reflects the subdued characteristics of the old landslides. Both Schulz (2004) and Haugerud *et al*. (2003) noted that aerial photographs are more effective in detecting small landslides, active shortly before the photos were taken. In a study by Gold (2004), also carried out near Seattle, independent landslide inventories developed from LIDAR and API were compared. No significant difference between the methods were found. In both cases about 60 per cent of the indicated sites were classified as real landslides after a field check. Finally, in contrast to the previous studies, McKean and Roering (2004) and Glenn *et al*. (2006) used the local surface roughness measured from LIDAR-derived high resolution DEMs to identify different morphological components within isolated landslides objectively. They both observed differences in surface roughness throughout the different parts of a landslide (i.e. high surface roughness and slope gradients in erosion zone, and low surface roughness in the landslide body). These differences in surface roughness within landslides suggest that the creation of a quantitatively derived regional landslide inventory is probably not straightforward, especially when investigating old earth slides with a subdued morphology which are characteristic of the Flemish Ardennes. All previous studies suggest that LIDAR is useful for identifying and delineating old landslides in densely forested areas. LIDAR-derived maps are easy to use both inside and outside (e.g. during a field check), and require less training than using aerial photographs. Although the creation of the LIDAR maps requires powerful computers and GIS software, the topographic data are easy to manipulate.

For the LIDAR data used in this study, flights took place in 2001 and 2002. An Azimuth Aeroscan small footprint (30 cm) multi-return LIDAR system with a pulse rate of 15 kHz and accuracy (RMSE) of 4 cm was used. The area of interest was flown at *c*. 1200 m a.s.l. Laser pulses generally were uniformly spaced within 600 m wide swaths with average pulse density of 1 per 4 m^2. Adjacent flight lines had a 30 per cent overlap, and for each block of flight lines at least two cross-flight-lines were measured. Reference fields were located within these cross-flight-lines. The last return from each pulse was assumed to be from the ground surface, although this was not always the case. The post-processing was conducted by the vendor. Creation of the bald earth DEM required the use of algorithms from the commercially available Terrascan software to automatically remove undesired returns. A manual check followed. Finally, flight lines were assembled using algorithms defined by the vendor. The database provided (DEM of Flanders, 2005) has a uniform point density of at least 1 per 20 m^2. The accuracy of the altitude depends on the soil cover and decreases with increasing vegetation heights. For forests and pastures an average vertical accuracy of at most 20 cm is assured, and for freshly cut lawns 7 cm (GIS-Vlaanderen, 2003).

LIDAR-derived maps and expert knowledge

A DEM with a 5 m resolution was derived from the LIDAR data using TIN interpolation. In order to remove production artefacts low pass filtering was applied. Using standard routines in the GIS software IDRISI (Kilimanjaro), a slope map, contour line map and two hillshade maps were created from the DEM. For the contour line map a 2 m interval was chosen, and for the two hillshade maps a sun elevation angle (i.e. slope angle of the illumination source above the horizon) of 30° and a sun azimuth angle (i.e. angle from which the light source is projected) of 315° and 45°. For the latter maps, no vertical exaggeration was used.

The identification of landslides on hillshade and contour line maps is based on the recognition of landslide characteristics (e.g. main scarps, reverse slopes, convex landslide foots) and alterations of the drainage system (e.g. a main valley stream pushed away by a landslide; Wills and McCrink, 2002). Expert knowledge is therefore indispensable to indicate landslides on hillshade and contour line maps. In order to assess the magnitude of interpretation differences

between experts, seven experts were asked to digitize the presumed landslides on a vector map which could be overlain on the hillshade, contour and slope maps in IDRISI. These same seven experts had, in an earlier study (Van Den Eeckhaut *et al.*, 2005), tested an alternative (i.e. faster and cheaper compared to field mapping) mapping technique, based on the interpretation of 1:100 000 hillshade maps derived from a 1:10 000 topographical map with a 2·5 m contour interval. The hillshade maps were created from a 5 m resolution DEM based on the digitized contours, and had similar illumination characteristics as those used in this analysis. The landslide mapping by experts based on these 1:100 000 hillshade maps did not result in a landslide inventory map of acceptable quality as only a few large landslides mapped in the field were identified on the hillshade maps (Van Den Eeckhaut *et al.*, 2005). Nevertheless, the important point here is that landslide inventories based on expert analysis using LIDAR-derived data (this study) can be compared directly with expert delineated landslide inventories based on topographic data extracted from large-scale maps (Van Den Eeckhaut *et al.*, 2005).

Presumed landslides had to be digitized as closed polygons including the whole affected area from the main scarp to the landslide foot. As an example, one landslide was already indicated on the vector map provided to the experts (Figure 1). Because all experts were familiar with hillshade, contour line and slope maps, no further training on the recognition of landslides was provided. The analysis of the maps and the indication of the presumed landslides took about two to four hours. Generally, presumed landslides were digitized at scales between 1:4000 and 1:10 000. Based on their familiarity with the study area, the experts were grouped into two familiar (experts 1 and 2) and five unfamiliar (experts 3 to 7) experts. The latter had visited the study area at most once, whereas familiar expert 1 is one of the two geomorphologists involved in the field survey, and familiar expert 2 helped to delineate and classify some of the less clear landslides. Although the familiar experts knew the location of a considerable number of the landslides mapped in the field, they indicated all hillslope sections for which they recognized landslide characteristics on the LIDAR-derived maps.

For the evaluation of the landslide inventory maps, polygon- and pixel-based approaches were used. Apart from the landslide inventory maps produced by the seven experts, combination maps of the two familiar, the five unfamiliar and all seven experts were made. The evaluation parameters used are explained in Table II. The positional mismatch (*PM*, per cent), was introduced by Carrara *et al.* (1992) for comparing quantitatively different landslide inventory maps of one study area.

For comparing the field survey with a LIDAR-based inventory, *PM* is calculated as:

$$PM = \left[\frac{NP_{F \cup Ei} - NP_{F \cap Ei}}{NP_{F \cup Ei}} \right] \times 100 \tag{1}$$

where $\cap$ and $\cup$ are the symbols for the intersection and union, respectively, of two maps, $NP_{F \cup Ei}$ is the number of pixels indicated as a landslide either in the field or/and by expert *i*, and $NP_{F \cap Ei}$ is the number of field landslide pixels indicated by expert *i*.

Similarly, for comparing two LIDAR-based inventories, *PM* is calculated as:

$$PM = \left[\frac{NP_{Ei \cup Ej} - NP_{Ei \cap Ej}}{NP_{Ei \cup Ej}} \right] \times 100 \tag{2}$$

where $NP_{Ei \cup Ej}$ is the number of pixels indicated as a landslide by expert *i* or/and expert *j*, and $NP_{Ei \cap Ej}$ is the number of pixels indicated as a landslide by expert *i* and expert *j*.

PM ranges between 100 per cent (no match) and 0 per cent (exact match) but generally has values between 50 and 70 per cent (Carrara *et al.*, 1995; Ardizzone *et al.*, 2002). In this study *PM* represents the total error and uncertainty associated with (1) the landslide identification by the experts both in the field and with the LIDAR-derived maps, and (2) the landslide indication on the topographical map during the field survey and on the digital LIDAR-derived maps during this experiment.

Results and Discussion

Internal morphology of landslides on LIDAR-derived hillshade maps

In contrast to the 1:100 000 hillshade maps based on the contour lines of the 1:10 000 topographical map used in Van Den Eeckhaut *et al.* (2005; Figure 2A), the internal morphology of the deep-seated landslides is clearly visible on the

Table II. Comparison parameters for evaluating the results of landslide (LS) mapping using the LIDAR-derived maps. For the pixel-based approach a 5 m resolution is used

	Field survey	
N_F	Number of field LS	All the LS mapped during the field survey
A_F	Total area of field LS	The sum of the areas of the field LS (ha)
NP_F	Number of field LS pixels	All the pixels located within one of the field LS
	Expert knowledge applied to LIDAR-derived maps	
	Polygon-based approach	
N_{Ei}	Number of presumed LS indicated by expert i	All the sites indicated by expert i on the hillshade, slope or contour line maps
A_{Ei}	Total area of presumed LS indicated by expert i	The sum of the areas of the presumed LS indicated by expert i (ha)
$N_{F \cap Ei}$	Number of field LS indicated by expert i	The field LS, located at least for one-half within an area indicated as a presumed LS by expert i. Several field LS can be located within one presumed LS. This explains why $N_{F \cap Ei}$ can be larger than N_{Ei}
$N_{E \setminus F}$	Number of additional LS indicated by expert i	The presumed LS indicated by expert i, which do not contain a field LS
$(N_{F \cap Ei}/N_F) \times 100$	Percentage of indicated field LS	For expert i, the ratio of the number of indicated field LS to the total number of field LS (%)
	Pixel-based approach	
NP_{Ei}	Number of presumed LS pixels, indicated by expert i	All the pixels located within one of the presumed LS indicated by expert i
$NP_{F \cap Ei}$	Number of field LS pixels indicated by expert i	All the pixels located within one of the field LS indicated by expert i
$(NP_{F \cap Ei}/NP_F) \times 100$	Percentage of indicated field LS pixels	For expert i, the ratio of the number of indicated field LS pixels to the total number of field LS pixels (%)
PM	Positional mismatch	Index of disagreement between the field survey-based and the LIDAR-based LS inventories or between LIDAR-based LS inventories of experts i and j (%)

$\cap$ and $\cup$ are the symbols for the intersection and union, respectively, of two maps.

LIDAR-derived hillshade map (Figures 2B, C and 3). Figure 2B shows two multiple rotational earth slides, both located under forest with the main scarps and several reverse slopes clearly distinguishable. The main scarps are indicated in white, because they are orientated to the light source located in the northwest. The reverse slopes of the southern landslide, which are orientated towards the east and thus lying in the shadow, are dark grey. A ditch draining ponding water from the highest reverse slope is also visible, and the curved form of the brook at the foot of the landslides indicates that it has been pushed to the west by the displaced slope material. Other examples of landslides, representative of the study area, are presented in Figure 3. On a hillshade map of a recently reactivated landslide (Figure 3A), the main scarp and drainage ditches evacuating the water exfiltrating at the base of the main scarp are clearly visible. Apart from individual landslides, some hills are marked by a concatenation of landslides (Figure 3C). These excerpts of the hillshade map all show that the toes of old landslides are more difficult to delineate than the main scarps, which reinforces both the findings of Schulz (2004) and the hypothesis that in our study area the creation of a quantitative inventory is not straightforward. It is important to note that these examples suggest that LIDAR images enable the determination of the morphological characteristics (total affected area, landslide length and width, height of main scarp, average hillslope gradient of affected area) and the classification of the landslides.

Consistency of LIDAR-based landslide inventories

The overall spatial distribution of the presumed landslides is fairly similar on all maps (Figure 4). The maps of experts 5 and 6 differ most. When a hillslope was affected by several landslides, expert 5 often indicated the entire area, including stable zones between landslides, as one unstable area. On the other hand, expert 6 indicated rather small presumed landslides. This also explains the large difference in number of presumed landslides (i.e. between 48 and 123; Table III).
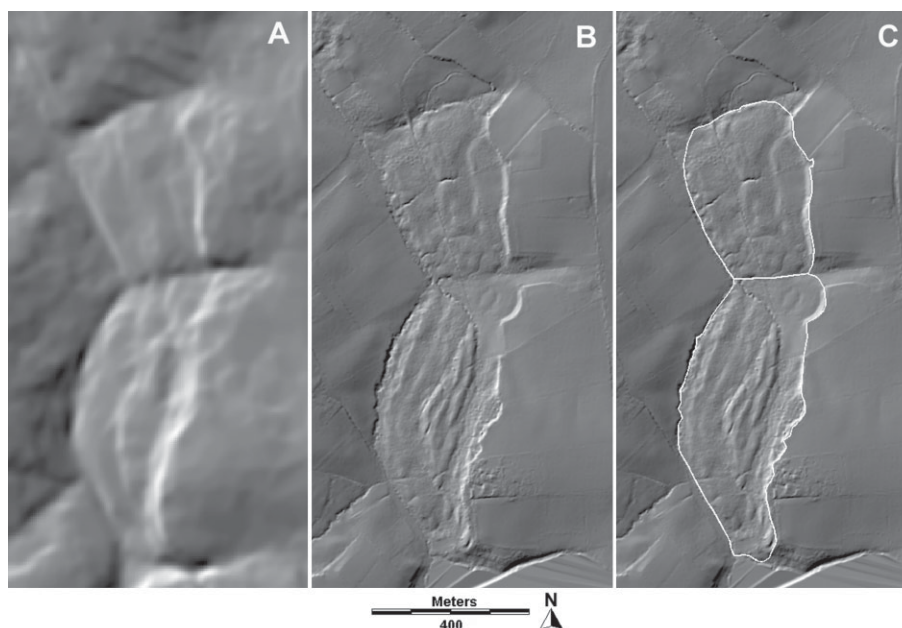
Figure 2. (A) Excerpt of hillshade map (Terrijst Forest, Maarkedal) derived from contour lines on the topographical map (1:10 000; NGI, 1972). (B) Same excerpt of LIDAR-derived hillshade map. (C) Same excerpt as (B) but with indication of two rotational earth slides both located under forest. Note the multiple reverse slopes of the southern landslide on (B) and (C).

Table III. Results from the field survey and from expert knowledge applied to LIDAR-derived hillshade, slope and contour line maps in a GIS environment (see Table II for the definition of the parameters)

	N_{Ei}	$N_{F \cap Ei}$	A_{Ei} (ha)	$(N_{F \cap Ei}/N_F) \times 100$ (%)	NP_{Ei}	$NP_{F \cap Ei}$	$(NP_{F \cap Ei}/NP_F) \times 100$ (%)
Field survey	77	77	350		138 345		
Expert							
1	84	72	429	93·5	171 407	114 695	82·9
2	70	61	458	79·2	183 048	104 140	75·3
3	99	63	278	81·8	111 234	81 529	58·9
4	123	67	354	87·0	141 509	85 711	62·0
5	50	57	744	74·0	297 451	97 537	70·5
6	61	38	116	49·4	45 174	27 935	20·2
7	48	48	366	62·3	146 318	79 293	57·3
Familiar*	97‡	72	556	93·5	222 450	121 015	87·5
Unfamiliar†	121‡	76	966	98·7	386 508	124 320	89·9
All	128‡	77	1038	100·0	415 154	129 473	93·6

* Familiar experts 1 and 2 involved in the creation of the field-survey based landslide inventory.

† Unfamiliar experts 3 to 7 who visited the study area at most once.

‡ It is possible that some of the presumed landslides in the combination maps are indicated as two or more individual, neighbouring presumed landslides on the landslide inventory maps of the individual experts.

Although the field survey-based landslide inventory is most probably not complete, it is considered to be the best approximation of the true landslide inventory. If LIDAR-derived maps are appropriate for mapping landslides, then a good expert should indicate most of the field landslides. Therefore the percentage of indicated field landslides ($N_{F \cap Ei}/N_F$) is the first important evaluation parameter. For all experts this parameter varies between 50 and 93 per cent (Table III). The ratio of the number of indicated field landslides to the total number of field landslides (i.e. column 4) and the ratio of the number of correctly indicated field landslide pixels to the total number of field landslide pixels
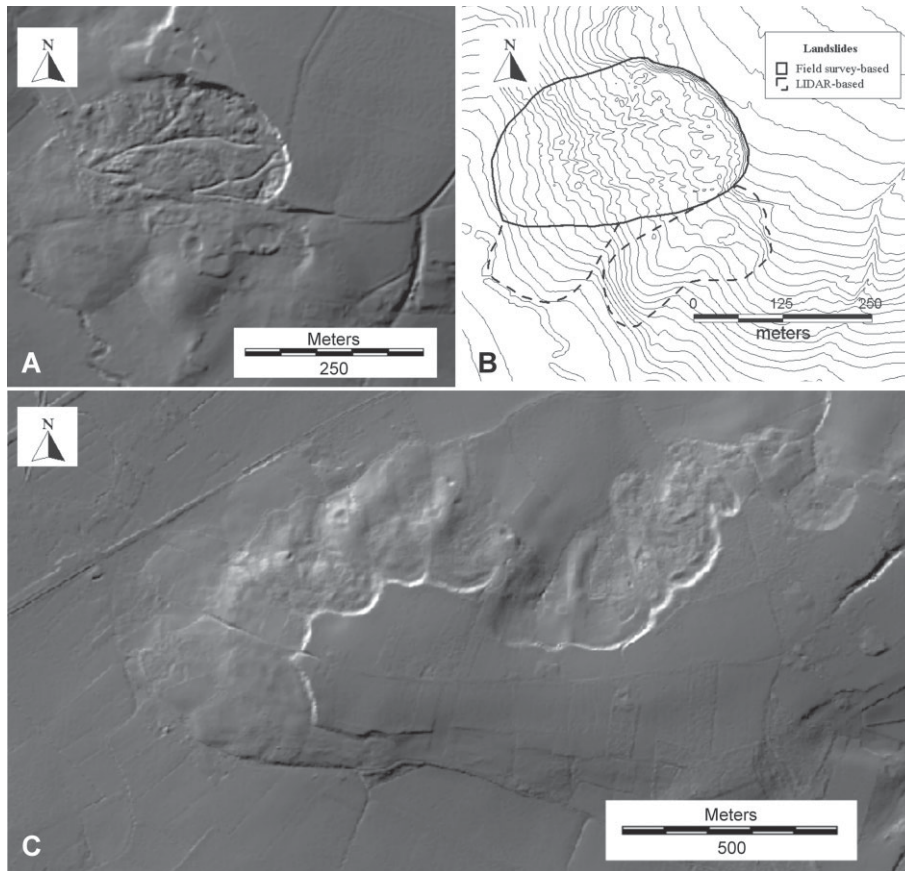
Figure 3. (A) Excerpt of LIDAR-derived hillshade map showing an active rotational earth slide with a curved main scarp (Hekkebrugstraat landslide; Oudenaarde). (B) Same excerpt as (A) of the LIDAR-derived contour line map with a 2 m interval. The boundaries of the active rotational earth slide as mapped in the field are drawn in a solid line. Analysis of LIDAR images resulted in a correction of the mapped boundaries of this active landslide, and in addition of a landslide not detected during the field survey (indicated with dotted line). (C) Excerpt of LIDAR-derived hillshade map showing a hill marked by a concatenation of landslides. About half of the landslides are located under forest (Rotelenberg-Koppenberg; Oudenaarde).

(i.e. column 7) illustrate the sometimes large differences (up to 29 per cent) between the polygon- and pixel-based approaches. These differences are due to the fact that for the pixel-based approach, all pixels were taken into account, whereas for the polygon-based approach a landslide was considered to be correctly indicated when at least half of the landslide, especially the depletion area, was indicated. Hence, differences in delineation of landslide boundaries were not taken into account. When combining the landslide inventory maps of the seven experts, all 77 field landslides were indicated. The area indicated as presumed landslides, however, is 1040 ha or 8·3 per cent of the study area. This is approximately three times the area affected by the field landslides. It is important to note that six large presumed landslides indicated only by expert 5 account for about one-third of this total area. Table IV provides information on the number of field landslides that were indicated by different experts. In total, 65 of the 77 landslides were indicated by at least four experts. The freshest landslides were most easily visible on the LIDAR-derived maps, because from the 27 landslides indicated by all experts there are 15 type 1 and eight type 2 landslides, whereas from the 12 field landslides indicated by less than four experts, there were five type 3 landslides and three possible landslides.

Large variations, between 116 and 744 ha, for the total indicated area (A_{Ei}, Table III), suggest that, apart from the percentage of indicated field landslides, this parameter has to be included in the evaluation of the quality of the LIDAR-based landslide maps. Landslide area is represented in the positional mismatch (*PM*). When comparing maps of the same area, but produced by different experts, *PM* has been found to range between 70 and 50 per cent (Ardizzone *et al*., 2002). In this study, two landslide inventory maps were therefore considered as comparable if they

Table IV. Distribution of the 77 field landslides indicated by *n* (*n* = 1, 2, . . . 7) experts and by landslide freshness. For rotational and complex earth slides, landslide freshness or preservation of the typical landslide characteristics decreases from type 1 to type 3 landslides

| Total number of experts	Landslide freshness			Possible landslide	Total	
	Type 1	Type 2	Type 3		Absolute	Relative
7	15	8	4	0	27	35·1
6	3	5	3	3	14	18·2
5	2	6	6	1	15	19·5
4	2	2	4	1	9	11·7
3	1	1	1	0	3	3·9
2	0	2	2	0	4	5·2
1	0	0	2	3	5	6·4
Total	23	24	22	8	77	100·0
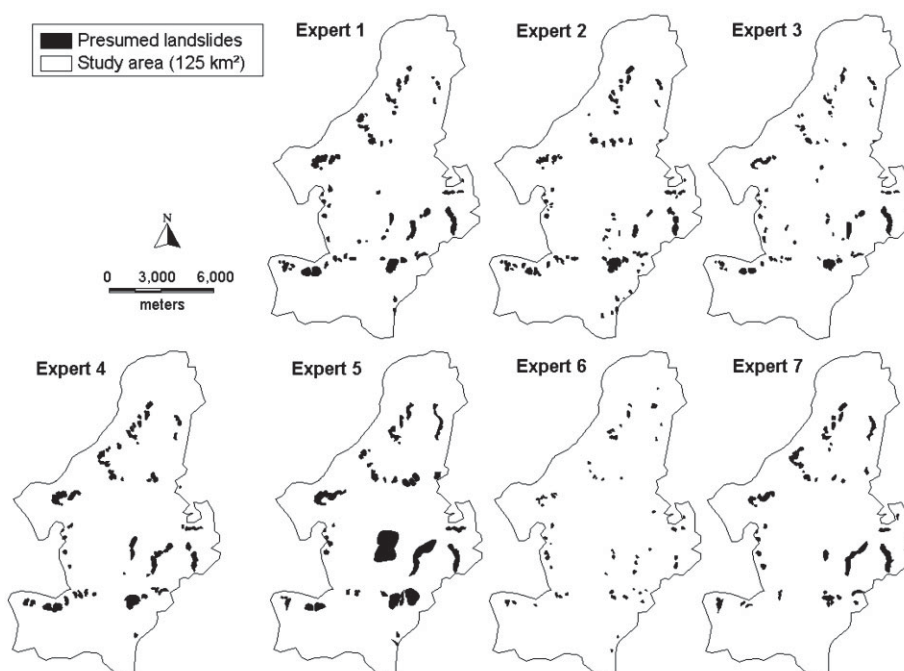
Figure 4. Landslide inventory maps based on the application of expert knowledge to LIDAR-derived hillshade, slope and contour line maps in a GIS environment.

had *PM* values less than an arbitrary threshold of 70 per cent. First, the field survey-based landslide inventory was successively compared with the maps of the experts (Table V). Apart from experts 5 and 6, all experts had values lower than 70 per cent, and created inventories comparable to the field survey-based inventory. In a second step, comparisons among the seven experts were made (Table V). Again, the upper limit of 70 per cent was exceeded when the landslide inventory of expert 6, and sometimes that of expert 5, was taken into account. In all other cases *PM* ranged from 40 to 70 per cent.

Figure 5 illustrates the combination of the percentage of indicated field landslides and the positional mismatch. High-quality maps must indicate more than 70 per cent of the field landslides, and the comparison with the field survey-based landslide inventory must result in *PM* values less than 70 per cent. Experts 1, 2, 3 and 4, and the three combination maps satisfy both criteria, whereas the maps produced by experts 5 and 7 are classified as being of moderate quality as they satisfy only one of the two criteria. Not satisfying one of the two criteria, the map created by expert 6 is considered to be low quality. The fact that the maps of the familiar experts 1 and 2 and the unfamiliar

Table V. Positional mismatch (*PM*, See Table II, and Equations 1 and 2 for definition of) calculated for the pairwise comparison of the field survey-based and LIDAR-based landslide inventory maps and for the comparison among the LIDAR-based inventory maps. *PM* values above the threshold of 70 per cent are given in italic, indicating that the maps are not comparable
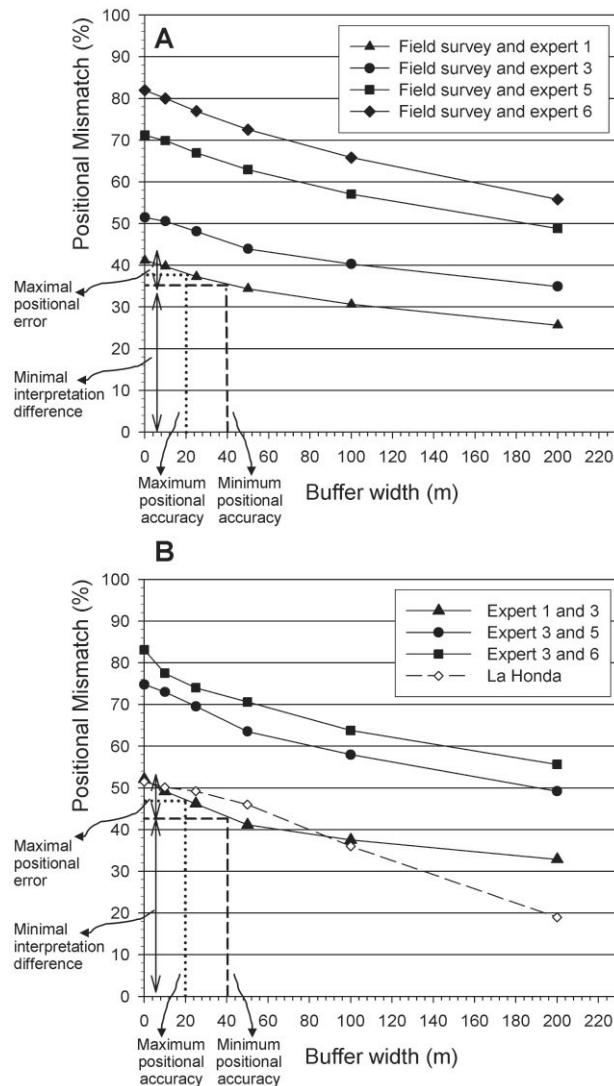
Positional mismatch (%)	Expert						
	1	2	3	4	5	6	7
Field survey	41·2	52·1	51·5	55·9	*71·2*	*82·0*	61·4
Expert							
1		40·7	50·7	48·3	65·6	*82·4*	56·2
2			56·9	55·1	61·2	*83·1*	56·0
3				55·8	*74·8*	*79·4*	59·5
4					*73·2*	*78·8*	63·2
5						*90·6*	69·2
6							*81·3*
7							
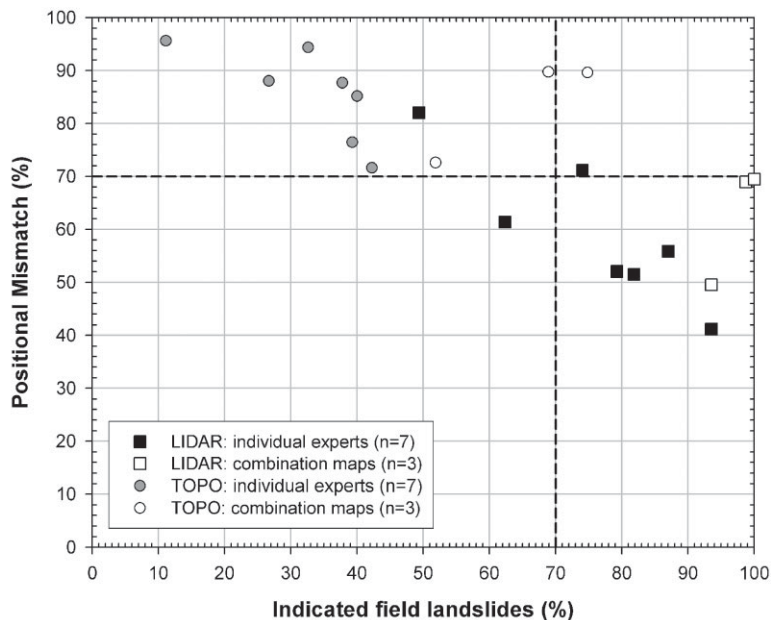
Figure 5. Positional mismatch between the field-based and expert-based landslide inventory maps by percentage of indicated field landslides (see Table II and Equation 1 for definitions of the parameters). In this study, high-quality inventory maps have a positional mismatch <70 per cent and a percentage of correctly indicated landslides >70 per cent. Dotted lines indicate these thresholds. (LIDAR = landslide inventory maps based on the application of expert knowledge to LIDAR-derived maps in a GIS environment; TOPO = landslide inventory maps based on expert knowledge applied to printed versions of 1:100 000 hillshade maps derived from the contour lines on the 1:10 000 topographical map).

experts 3 and 4 form one cluster in Figure 5 suggests that no intensive field visit is needed prior to the creation of LIDAR-derived landslide inventories.

In contrast with many other landslide inventory studies, an attempt is made to divide *PM* (i.e. total mapping error) into a part resulting from the interpretation differences of the geomorphologists who created both the field survey- and LIDAR-based landslide inventory maps, and into a part resulting from the positional error (from scale and accuracy of topographical and LIDAR-derived maps and from drawing and digitization on the topographical map). A method suggested by Carrara *et al*. (1992) was used. The field survey-based inventory and LIDAR-based inventory maps of experts 1, 3 (high quality), 5 (moderate quality) and 6 (lower quality) were selected, and successive buffers of 10, 25,

Figure 6. Estimated positional mismatch obtained by adding uncertainty, i.e. buffers of different widths to the indicated landslides. (A) Pairwise comparison of field survey- and LIDAR-derived landslide inventory. (B) Pairwise comparison of LIDAR-derived landslide inventories (La Honda = graph obtained by Carrara *et al.* (1992) from pairwise comparison of two landslide inventories derived from aerial photographs for the La Honda basin in California). Dotted and dashed lines indicate how positional error and interpretation differences can be estimated from the maximum (i.e. 20 m) and minimum (i.e. 40 m) positional accuracy, respectively. An example for minimum positional accuracy is shown in each graph.

50, 100 and 200 m were drawn around each digitized landslide. Then *PM* values were calculated by pairwise comparison of the five maps for each buffer size. All investigated pairs show the same trend (Figure 6): *PM* decreases with increasing buffer size. However, above a buffer of 50 m the rate of improvement decreases. Although the decrease in the first 50 m is opposite to the observations of Carrara *et al.* (1992; Figure 6B), we assume this is due to fact that positional errors are only important for the first few tens of metres around the boundaries, so that at higher distances the total mapping error consists mainly of interpretation differences. Hence, knowledge of the positional accuracy would enable to estimate that part of *PM* resulting from interpretation differences.

The positional accuracy of the field survey- and LIDAR-based inventory maps was estimated by measuring for each field landslide the maximum distance between (1) the main scarp as it was mapped in the field and the furthest drawn presumed landslide scarp corresponding to that field landslide, and (2) the two presumed landslide scarps corresponding to the same field landslide whose locations differed the most. The main scarp was chosen because we assumed

that, given the fact that the landslides were digitized at map scales between 1:4000 and 1:10 000, for most landslides the error due to interpretation differences would be least for this part of the landslide and thus the obtained distances would represent a first estimation of the positional accuracy. The average distance between the main scarp of each field landslide and its corresponding furthest located presumed landslide scarp was 22 (±16) m. Between the scarps of the two most different presumed landslides corresponding to the same field landslide, an average distance of 27 (±16) m was measured. So when taking a buffer of 40 m, all positional errors are assumed to be excluded. The corresponding *PM* of 35 per cent indicated in Figure 6A would only result from interpretation differences related to the use of different techniques, whereas the corresponding *PM* of 42 per cent indicated in Figure 6B would result from interpretation differences between experts 1 and 3. Overall, positional errors range between 6 and 12 per cent. When high-quality inventory maps (i.e. field survey, experts 1 and 3) are compared, interpretation differences range between 35 and 46 per cent, whereas this value can increase to 70 per cent for the lower quality maps. *PM* values found in similar studies (Carrara *et al*., 1995; Ardizzone *et al*., 2002) were located in between this range, and according to Carrara *et al*. (1992) a similar error magnitude is expected to be associated with many other geomorphological interpretations.

## Combination of field survey- and LIDAR-based landslide inventories: redundant or complementary

Table III shows that with the exception of expert 5, between 55 and 73 per cent of the total area of presumed landslides correspond with areas affected by a field landslide. This is comparable to the value of 60 per cent obtained by Gold (2004). Two important questions are now: did the remaining 27 to 45 per cent contain landslides not mapped during the field survey, and did the analysis of LIDAR-derived maps result in an improvement of the existing landslide inventory map? As mentioned before, API was not a good technique for the mapping of the landslides in the study area, because 75 per cent of the landslides were partly or completely covered by dense forest cover, and because of the subdued morphology of many of the large landslides. However, both limitations of API also affect the quality of the field survey-based inventory. As LIDAR can virtually look through vegetation, the first limitation is solved in this study. Another advantage is that analysing LIDAR-derived maps enabled the experts to have a complete overview of the large landslides. With these two advantages, the experts using LIDAR-derived maps might have either found landslides which were not observed during the field survey, or indicated presumed landslides in a better way compared to the field survey-based inventory.

In order to check this, a map was created distinguishing between presumed landslide pixels indicated by at least four and by less than four experts, respectively. Four experts were chosen because of the previous observation (Figure 5) that four experts created high-quality landslide inventory maps. A combination of this map with the field survey-based inventory (Figure 7) shows that in addition to the 350 ha indicated as affected in the field, 89 ha were indicated by at least four experts and 623 ha by at most three experts. Ten landslides, which were not mapped during the field survey, were indicated by at least four experts. These new landslides were probably not identified in the field because the affected area was hardly accessible (private property, $n = 3$) and/or because of the dense forest cover or human interference ($n = 7$). Besides the identification of new landslides, the boundaries of 11 field landslides were corrected (Figures 7, 3A and B), because the landslide boundaries indicated by four or more experts differed considerably from the boundaries mapped in the field. These corrections, all located in the accumulation zone of the landslides, do not include small changes of 5 to 10 m. During the field survey, apparently only the most distinct, freshest parts of these landslides were mapped (e.g. Figure 3A and B).

Taken as a whole, these observations indicate that the analysis of the LIDAR images is complementary to the field survey. The combination of both methods can result in landslide inventory maps of high quality. A new landslide inventory of the test area was constructed by combining the results from the field survey with those from the analysis of LIDAR-derived maps by experts. The map contains 66 landslides (76 per cent) mapped in the field and indicated by at least one expert, 11 landslides (13 per cent) mapped in the field but corrected after analysing LIDAR images, and ten landslides (11 per cent) solely mapped from LIDAR images. Similar to Figure 7, the sites indicated by at least one expert are shown on the map.

Our study is one of the few where a field survey preceded the interpretation of the LIDAR images. However, the combination of both techniques will more effectively produce high-quality landslide inventory maps in hilly forested regions. First the LIDAR-derived maps should be analysed, if possible by more than one expert, using hillshade, slope and contour line maps in combination with slope profiles. Afterwards a field check is indispensable as this study has shown that not all presumed landslide areas indicated on the map are true landslides. Apart from identifying and delineating landslides, the experts can also gain additional information from the maps, such as the morphological characteristics or type of the landslides. As Keaton and Degraff (1996) provide characteristic block diagrams for each
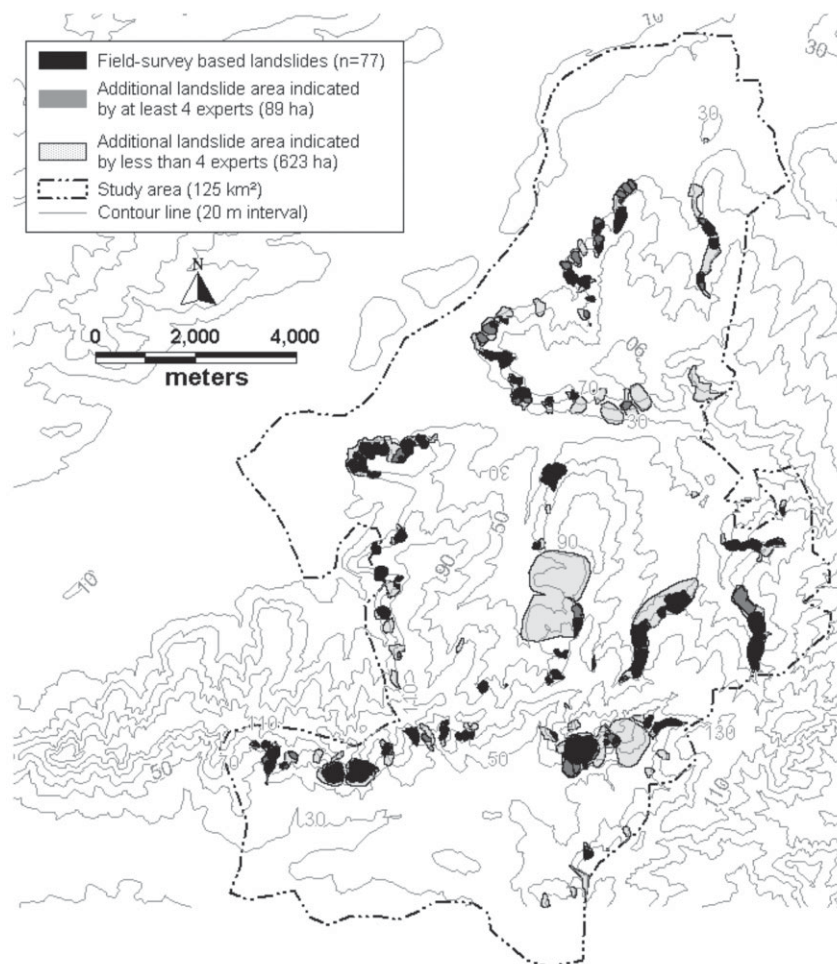
Figure 7. Landslide inventory of the study area combining the results from the field survey and from the analysis of the LIDAR-derived maps.

landslide activity state, ranging from active to dormant/old, comparison of these block diagrams with the hillshade maps also allows the determination of the activity state for each landslide.

Comparison with results of Van Den Eeckhaut *et al.* (2005)

As mentioned before, the same seven experts were asked to indicate presumed landslides on a printed version of two 1:100 000 hillshade maps derived from the contour lines (2·5 m interval) of the topographical map (1:10 000; NGI, 1972) during a comparable study carried out by Van Den Eeckhaut *et al.* (2005). The evaluation parameters of these topographic-based inventory maps (Table VI) are presented for the complete 430 km^2 study area. The experts indicated only 15 to 57 of the 135 field landslides. Total indicated areas (A_{Ei}) ranged from 161 to 1523 ha, being respectively about three times lower and three times higher than the total affected area mapped in the field (i.e. 562 ha). The positional mismatch (*PM*) between the field-based and expert-based landslide inventories ranged from 71·6 to 95·6 per cent. To enable a comparison between the topographic- and LIDAR-based maps, the results of Van Den Eeckhaut *et al.* (2005) were added to Figure 5. Results of the maps created during the two studies are located in two distinct clusters. The observed differences are explained by the different quality of the topographic data, the different mapping scales (i.e. 1:100 000 versus 1:4000 to 1:10 000) and the different mapping technique (i.e. drawing on paper version of hillshade map versus direct digitization in GIS environment). The topographic-derived landslide inventory maps are located in the upper left corner of the graph. They all have values for *PM* larger than the threshold of 70 per cent and percentages of indicated field landslides lower than 50 per cent. These poor results reinforce the

Table VI. Results from Van Den Eeckhaut *et al.* (2005): expert knowledge applied to printed versions of 1:100 000 scale hillshade maps derived from contour lines on a 1:10 000 topographical map (see Table II for the definition of the parameters)

	$N_{F \cap Ei}$	A_{Ei} (ha)	$(N_{F \cap Ei}/N_F) \times 100$ (%)	NP_{Ei}	$NP_{F \cap Ei}$	$(NP_{F \cap Ei}/NP_F) \times 100$ (%)	PM (%)
Field	135	562		225 029			
Expert							
1	57	423	42·2	140 003	74 437	41·2	71·6
2	53	572	39·3	199 735	83 774	40·8	76·5
3	54	1114	40	272 278	72 826	41·0	85·2
4	51	1115	37·8	257 329	41 990	34·8	87·7
5	44	1523	32·6	610 599	44 554	21·1	94·4
6	15	161	11·1	52 457	11 462	5·7	95·6
7	36	501	26·7	200 269	45 380	21·5	88·1
Familiar*	70	790	51·9	270 384	109 384	55·0	72·6
Unfamiliar†	93	3357	68·9	1 146 134	127 766	68·9	89·8
All	101	3537	74·8	1 236 227	154 556	73·7	89·6

* Familiar experts 1 and 2 involved in the creation of the field-survey based landslide inventory.
† Unfamiliar experts 3 to 7 who visited the study area at most once.

conclusions of Van Den Eeckhaut *et al*. (2005) that the analysis of hillshade maps produced from contour lines on the topographical map could not replace detailed field surveys.

Conclusions

The problem of mapping old landslides under forest has been reported for many landslide-prone areas all over the world. In this study, LIDAR data were tested for the creation of a landslide inventory map for a 125 km^2 area in the Flemish Ardennes, a hilly area affected by old landslides with a subdued morphology. The magnitude of interpretation differences among geomorphologists was also investigated. Seven experts, experienced in landslide mapping, individually created a landslide inventory by indicating presumed landslides on LIDAR-derived hillshade, slope and contour line maps in a GIS environment. High-quality landslide inventory maps were separated from lower quality maps by pairwise comparison of each of the seven maps with the other six, and with a detailed field survey-based landslide inventory carried out before the LIDAR data became available. For this study, high-quality LIDAR-derived landslide inventory maps contained 70 per cent of the landslides mapped during the field survey and they had a mapping error (expressed as the positional mismatch) of less than 70 per cent when compared with the field survey-based inventory. These two criteria were met by four experts. Although landslides are more difficult to identify with decreasing landslide freshness, the observation that values of *PM* among the experts are generally (i) of the same order as *PM* values obtained when comparing the field survey-based with each expert-based landslide inventory maps, and (ii) below our threshold of 70 per cent, suggests that the analysis of LIDAR images is an appropriate technique to map landslides in hilly and densely forested regions.

Whereas other studies suggested that the interpretation of aerial photographs and LIDAR images are complementary tools in landslide inventory mapping, this analysis showed that detailed field surveys and analysis of LIDAR images are complementary. For the study area, the combined use of the two methods resulted in a new inventory map with: (1) landslides correctly mapped in the field and also indicated by at least one expert (76 per cent); (2) landslides incorrectly mapped in the field but corrected after analysing the LIDAR images (13 per cent); and (3) landslides only identified on the LIDAR images (11 per cent). Finally, separation of the differences resulting from the experts' interpretations and from the positional error suggested that, for the four high-quality LIDAR-derived landslide inventory maps and for the field survey-based landslide inventory, drawing a 40 m buffer around the landslide boundaries seemed appropriate to exclude most positional errors, and to estimate interpretation differences of between 35 and 46 per cent.

The results of the present study revealed that for hilly regions affected by old landslides, high-quality landslide inventory maps can be obtained through the combination of the analysis of LIDAR-derived maps in a GIS environment, where possible by different experts, and detailed field checks. This method is recommended for all areas affected by landslides under forest.

Acknowledgements

References

Ardizzone F, Cardinali M, Carrara A, Guzzetti F, Reichenbach P. 2002. Impact of mapping errors on the reliability of landslide hazard maps. *Natural Hazards and Earth System Sciences* **2**: 3–14.

Carrara A, Cardinali M, Detti R, Guzzetti F, Pasqui V, Reichenbach P. 1992. GIS techniques and statistical models in evaluating landslide hazard. *Earth Surface Processes and Landforms* **16**: 427–445.

Carrara A, Cardinali M, Guzzetti F, Reichenback P. 1995. GIS technology in mapping landslide hazard. In *Geographical Information Systems in Assessing Natural Hazards*, Carrara A, Guzzetti F (eds). Kluwer: Dordrecht; 135–176.

Carter W, Shrestha R, Tuell G, Bloomquist D, Sartori M. 2001. Airborne Laser Swath mapping shines new light on earth's surface. *Eos, Transactions, American Geophysical Union* **82**: 549, 550, 555.

Crozier JM. 2005. Management frameworks for landslide hazard and risk: Issues and options. In *Landslide Hazard and Risk*, Glade T, Anderson M, Crozier MJ (eds). John Wiley and Sons: Chichester; 331–350.

Cruden DM, Varnes DJ. 1996. Landslide Types and Processes. In *Landslides, Investigation and Mitigation, Transportation Research Board*, Turner AK, Schuster RL (eds). National Research Council, Special Report 247. National Academy Press: Washington, DC; 36–71.

DEM of Flanders. 2005. MVG-LIN-AWZ and MVG-LIN-AMINAL (GIS-Vlaanderen). http://www.gisvlaanderen.be/gis/diensten/geo-vlaanderen/?artid=240 [10 January 2006].

Demoulin A, Pissart A, Schroeder C. 2003. On the origin of late Quaternary paleolandslides in the Liège (E Belgium) area. *International Journal of Earth Science* **92**: 795–805. DOI: 10.1007/s00531-003-0354-7.

GIS-Vlaanderen. 2003. *Nieuwsbrief GIS-Vlaanderen: Digitaal Hoogtemodel Vlaanderen*. Ondersteunend Centrum GIS-Vlaanderen: Gent. http://www.gisvlaanderen.be/gis/diensten/geo-vlaanderen/?artid=240

Glenn NF, Streutker DR, Chadwick J, Glenn DJ, Thackray GD, Dorsch SJ. 2006. Analysis of LiDAR-derived topographic information for characterizing and differentiating landslide morphology and activity. *Geomorphology* **73**: 131–148. DOI: 10.1016/j.geomorph.2005.07.006.

Gold RD. 2004. *A Comparative Study of Aerial Photographs and LIDAR Imagery for Landslide Detection in the Puget Lowland, Washington*. Washington Division of Geology and Earth Resources. Open File Report 2004-6.

Guzzetti F, Cardinali M, Reichenbach P, Carrara A. 2000. Comparing landslide maps: a case study in the Upper Tiber River Basin, Central Italy. *Environmental Management* **25**: 247–263. DOI: 10.1007/s002679910020.

Haneberg WC. 2005. The ins and outs of airborne LIDAR: An introduction for practicing engineering geologists. *AEG news* **48**: 16–19.

Haneberg WC, Creighton AL, Medley EW, Jonas DA. 2005. Use of LIDAR to assess slope hazards at the Lihir gold mine, Papua New Guinea. *Proceedings of 2005 International Conference on Landslide Risk Management*, Vancouver, May/June 2005.

Haugerud RA, Harding DJ, Johnson SY, Harless JL, Weaver CS, Sherrod BL. 2003. High resolution LIDAR topography of the Puget Lowland, Washington – a bonanza for earth science. *GSA Today* **13**: 4–10.

Hodgson ME, Jensen JA, Schmidt L, Schill S, Davis B. 2003. An evaluation of LIDAR- and IFSAR-derived digital elevation models in leaf-on conditions with USGS Level 1 and Level 2 DEMs. *Remote Sensing of Environment* **84**: 295–308.

IAEG Commission on Landslides. 1990. Suggested nomenclature for landslides. *Bulletin of the International Association of Engineering Geology* **41**: 13–16.

IWONL. 1987. *Text Clarifying the Belgian Soil Map, Map Sheet 98E Ronse (in Dutch)*. Uitgegeven onder de auspiciën van het Instituut tot aanmoediging van het Wetenschappelijk onderzoek in Nijverheid en Landbouw: Brussels.

Jacobs P, De Ceukelaire M, De Breuck W, De Moor G. 1999. *Text Clarifying the Belgian Geological Map, Flemish Region, Map Sheet 29 Kortrijk, Map Scale 1/50 000 (in Dutch)*. Ministerie van Economische zaken en Ministerie van de Vlaamse Gemeenschap: Brussels.

Keaton JR, DeGraff JV. 1996. Surface observation and geologic mapping. In *Landslides, Investigation and Mitigation, Transportation Research Board*, Turner AK, Schuster RL (eds). National Research Council, Special Report 247. National Academy Press: Washington, DC; 128–230.

McKean J, Roering J. 2004. Objective landslide detection and surface morphology mapping using high-resolution airborne laser altimetry. *Geomorphology* **47**: 331–351. DOI: 10.1016/S0169-555X(03)00164-8.

Metternicht G, Hurni L, Gogu R. 2005. Remote sensing of landslides: An analysis of the potential contribution to geo-spatial systems for hazard assessment in mountainous environments. *Remote Sensing of Environment* **98**: 284–303. DOI: 10.1016/j.rse.2005.08.004.

NGI (National Geographical Institute), 1972. *Topographical map of Belgium (1:10 000)*. Sheets 29/3-4-7-8 and 30/1-2-5-6. National Geographical Institute: Brussels.

Ost L, Van Den Eeckhaut M, Poesen J, Vanmaercke-Gottigny MC. 2003. Characteristics and spatial distribution of large landslides in the Flemish Ardennes (Belgium). *Zeitschrift für Geomorphologie* **47**: 329–350.

Rowlands KA, Jones LD, Whitworth M. 2003. Landslide laser scanning: a new look at an old problem. *Quarterly Journal of Engineering Geology and Hydrogeology* **36**: 155–157.

Schulz WH. 2004. *Landslides mapped using LIDAR imagery, Seattle, Washington*. United States Geological Survey, Open File Report 2004–1396.

Schuster RL, Kockelman WJ. 1996. Principles of landslide hazard reduction. In *Landslides Investigation and Mitigation*, Turner AK, Schuster RL (eds). National Research Council, Special Report 247. National Academy Press: Washington, DC; 91–103.

Thoma DP, Gupta SC, Bauer ME, Kirchoff CE. 2005. Airborne laser scanning for riverbank erosion assessment. *Remote Sensing of Environment* **95**: 493–501. DOI: 10.1016/j.rse.2005.01.012.

Vanacker V, Vanderschraeghe M, Govers G, Willems E, Poesen J, Deckers J, De Bievre B. 2003. Linking hydrological, infinite slope stability and land-use change models through GIS for assessing the impact of deforestation on slope stability in high Andes watersheds. *Geomorphology* **52**: 299–315. DOI: 10.1016/S0169-555X(02)00263-5.

Van Den Eeckhaut M, Poesen J, Verstraeten G, Vanacker V, Moeyersons J, Nyssen J, Van Beek LPH. 2005. The effectiveness of hillshade maps and expert knowledge in mapping old deep-seated landslides. *Geomorphology* **67**: 351–363. DOI: 10.1016/j.geomorph.2004.11.001.

Vanmaercke-Gottigny MC. 1980. Landslides as a morphogenetic phenomenon in a hilly region of Flanders (Belgium). In *Assessment of Erosion*, De Bood M, Gabriel D (eds). John Wiley and Sons: Chichester; 475–484.

Vanmaercke-Gottigny MC. 1995. *Detailed geomorphological mapping as a scientific investigation method, a case study: the maps 'Geraardsbergen' and 'Kortrijk'*. PhD thesis, Faculty for Sciences, V.U.B., Brussels.

van Westen CJ, Seijmonsbergen AC, Mantovani F. 1999. Comparing landslide hazard maps. *Natural Hazards* **20**: 137–158. DOI: 10.1023/A:1008036810401.

White SA, Wang Y. 2003. Utilizing DEMs derived from LIDAR data to analyse morphologic change in the North Carolina coastline. *Remote Sensing of Environment* **85**: 39–47. DOI: 10.1016/S0034-4257(02)00185-2.

Wills CJ, McCrink TP. 2002. Comparing landslide inventories, the map depends on the method. *Environmental and Engineering Geoscience* **8**: 279–293.

Zêzere JL. 2002. Landslide susceptibility assessment considering landslide typology, a case study in the area north of Lisbon (Portugal). *Natural Hazards and Earth System Sciences* **2**: 73–82.